Journal of Experimental Nanoscience
Publication details, including instructions for authors and subscription information:
http://www.informaworld.com/smpp/title~content=t716100757

Novel flame-gradient method for synthesis of metal-oxide channels, nanowires and nanorods

Wilson Merchan-Merchan[a]; Alexei V. Saveliev[b]; Walmy Cuello-Jimenez[a]
[a] School of Aerospace and Mechanical Engineering, University of Oklahoma, Norman, OK 73019, USA
[b] Department of Mechanical and Aerospace Engineering, North Carolina State University, Raleigh, NC 27695, USA

First published on: 18 January 2010

To cite this Article Merchan-Merchan, Wilson , Saveliev, Alexei V. and Cuello-Jimenez, Walmy(2010) 'Novel flame-gradient method for synthesis of metal-oxide channels, nanowires and nanorods', Journal of Experimental Nanoscience, 5: 3, 199 — 212, First published on: 18 January 2010 (iFirst)
To link to this Article: DOI: 10.1080/17458080903464108
URL: http://dx.doi.org/10.1080/17458080903464108

Journal of Experimental Nanoscience
Vol. 5, No. 3, June 2010, 199–212

Taylor & Francis
Taylor & Francis Group

Novel flame-gradient method for synthesis of metal-oxide channels, nanowires and nanorods

Wilson Merchan-Merchan[a]*, Alexei V. Saveliev[b] and Walmy Cuello-Jimenez[a]

[a]*School of Aerospace and Mechanical Engineering, University of Oklahoma, Norman, OK 73019, USA;* [b]*Department of Mechanical and Aerospace Engineering, North Carolina State University, Raleigh, NC 27695, USA*

(*Received 1 September 2009; final version received 4 November 2009*)

The formation of 1D and 3D transition metal oxide (TMO) nano- and micron-size structures on molybdenum, iron and tungsten probes inserted in a counter-flow flame is studied experimentally. The unique thermal profile and chemical composition of the generated flame tends to convert almost pure bulk (99.9%) transition metal materials into 1D and 3D architectures. The synthesised Mo-, Fe- and W-oxide structures exhibit unique morphological characteristics. The application of Mo probes results in the formation of micron-size hollow and solid Mo-oxide channels. The formation of solid iron oxide nanorods is observed on iron probes. The use of W probes results in the synthesis of 1D solid carbon/metal oxide nanowires. This study confirms the existence of a common generic mechanism controlling the growth of the structures on the high-temperature probes. Metal oxide/hydroxides are formed on the probe surface exposed to the high-temperature oxidative environment. These oxides/hydroxides are further evaporated and transported by the gas flow to the low-temperature side where they are reduced to other oxide forms and deposited in the form of 1D or 3D TMO materials. This study reveals that a preferential growth at the edges of the MoO_2 whisker tips leads to the development of hollow structures.

Keywords: transition metal oxides; nanostructures; combustion synthesis; electron microscopy

1. Introduction

Flames have been successfully employed for the growth of a variety of nano- and micromaterials such as fullerenes [1–3], carbon nanotubes [4–12], carbon whiskers, diamond crystals and other nanomaterials such as carbides and oxides of various metals [13–19]. In recent years, much effort has been devoted to the study of transition metal oxides (TMOs) and related materials. The conversion of transition metals to corresponding oxide forms produces materials with distinct chemical, mechanical and electronic properties. A variety of uses facilitate the development of novel synthesis methods for the

*Corresponding author. Email: wmerchan-merchan@ou.edu

ISSN 1745–8080 print/ISSN 1745–8099 online

DOI: 10.1080/17458080903464108
http://www.informaworld.com

generation of unique 1D and 3D TMOs and related materials with desirable structure, chemical activity and physical properties.

Groups 3–12 of the periodic table are called transition metals and serve as a bridge, or transition, between the elements in the first two columns on the right and the 13th–18th columns on the left of the periodic table. The elements in groups 3–12 of the periodic table are metals; they are ductile and malleable, conduct electricity and heat as if possessing properties common to all metals. The valence electrons of transition metals are present in more than one shell, therefore, often exhibiting several common oxidation states. Despite many similarities, the transition metals do vary considerably in certain properties. There is a general decrease in the size of atomic radii from left to right for each of the series in the periodic table. There is a significant increase in atomic radius from 3d to 4d metals, although the 4d and 5d metals have remarkably similar atomic radii. Within the 3d, 4d and 5d blocks of the transition series, all of the metals form cubic and hexagonal crystal structures except Hg, which contains a rhombohedral structure. Some of these metals have very different melting points such as W at 3410°C and Hg as a liquid at −39°C. Transition metals such as Mo, Fe and Ti are hard and strong and make very useful structural materials; others such as Cu, Ag and Au are relatively soft and highly conductive.

It has been shown that molybdenum oxides possess unique catalytic and electronic properties and have potential applications in chemical synthesis, petroleum refining, recording media and sensors [14–16]. For catalytic application, several techniques have been developed to synthesise nanodispersed molybdenum oxides directly on alumina- and silica-support surfaces. A number of studies have been devoted to the growth of MoO_2 nanoparticles and wires on various substrates. For instance, Zhou et al. [20] have reported the formation of MoO_2 nanowire arrays by employing a high-temperature heating process in a vacuum chamber.

Iron oxides are widespread in nature and can be synthesised and structurally modified in the laboratory with controllable shapes and sizes for a variety of applications in electronics, medicine, chemistry and biology [21–24]. Recently, much attention has been given to the controlled synthesis of 1D iron oxide nanostructures [25–27] such as nanowires and nanorods. These materials have wide potential applications as catalysts, pigments, sensors, ferrofluids, magnetic recording and imaging materials. Fe-oxide nanorods, nanowires and nanotubes have been synthesised by various methods including aqueous chemistry, deposition in aluminium- and silicon-oxide templates and pulsed laser deposition [28].

Recent studies demonstrated that tungsten oxide materials possess unique photocatalyst, electrochromic, gaschromic and optochromic properties. Materials with these properties are key components in information displays, sensor devices and 'smart' windows [29]. Tungsten oxide possesses the interesting property of electrochromism, a permanent, reversible colour change under the application of electrical fields. Structures with pointy and elongated characteristics such as nanotubes, nanorods and microrods are considered to be excellent field emission electron sources, chiefly due to their high aspect ratio defined by the natural geometry of the 1D structures.

Different techniques have been proposed and developed for the synthesis of TMOs including aqueous chemistry [22], deposition in alumina- and silicon-oxide templates [25], pulsed laser deposition [30,31], high-temperature heating process in a restricted vacuum

chamber [32] and metal-organic vapour phase epitaxy [33]. Although these methods are capable of producing TMOs, they are generally limited by the complexity of the process, scalability and purity of the products. The volumetric production of nanopowders using flames is very attractive as a continuous-flow, scaleable, low-cost, one-step process. In this study, we report the synthesis of 1D and 3D transition metal oxide structures formed on high-purity metallic probes inserted in the high-temperature zone of an opposed flow oxygen-rich flame.

2. Experimental

Figure 1 shows the experimental setup used in the present study. A counter-flow burner forms two opposite streams of gases; the fuel (methane seeded with 4% of acetylene) is supplied from the top nozzle and the oxidiser (50% $O_2 + 50\%$ N_2) is introduced from the bottom nozzle. The top and bottom nozzles have inside diameters of 40 mm. A detailed description of the burner is given by Beltrame et al. [34]. The experiments were conducted with constant fuel and oxidiser velocities and a strain rate equal to $20\,s^{-1}$. Transition metal probes of high purity such as iron, molybdenum and tungsten were introduced into the flame through the tubular protecting shield. The position of the probe in the flame Z was measured from the top nozzle. Transmission electron microscope (TEM), scanning electron microscope (SEM), X-ray energy dispersive spectroscopy (EDS) and selected area electron diffraction (SAED) pattern microscopy were employed to characterise the structural and elemental composition of the synthesised structures.

3. Results and discussion

Transition metal probes of various types were tested for the bulk conversion of metals into 1D and 3D metal oxide structures through a flame probe interaction. The synthesis results are affected by two main factors: (1) structural and thermal properties of the tested probes and (2) the strong axial gradient of temperature and chemical species concentrations of the counter-flow flame.

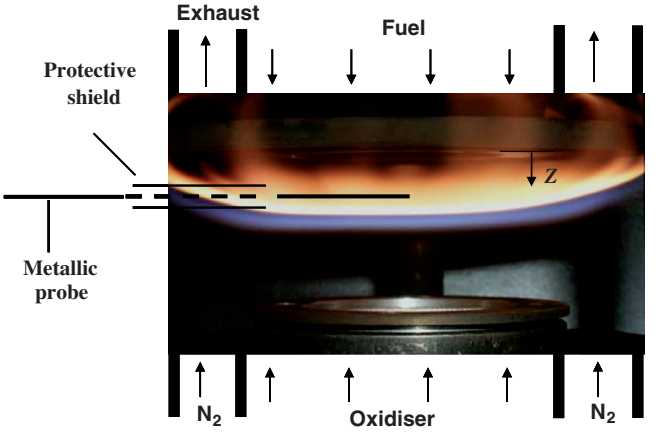

Figure 1. Schematic representation of the experimental setup.

3.1. *Synthesis of 3D Mo-oxide channels*

The introduction of a 1 mm Mo probe in the flame medium resulted in the formation of unique 3D micron-size structures. The 1 mm diameter molybdenum probe was exposed to the flame at a height of $Z = 11$ mm. Performed SEM analysis revealed that the surface of the probe is covered with densely packed micron-size whiskers in the form of hollow channels with rectangular cross-section (Figure 2). High-resolution SEM of the flame-exposed molybdenum probe showed that the formed structures are slender, prismatic and completely hollow with very large inside cavities devoid of other materials (Figure 2a and insert). The unique morphology with large cavities, nano thick walls, sharp edges and high specific surface area gives the structure a significant importance, for example, in medical applications. The large cavities can also be used for a wide variety of applications such as the storage of fluids or nanoparticles, material reinforcements or as a component in the fabrication of MEMs devices, etc. Figure 2 clearly shows the high aspect ratio between the thickness of the walls of a rectangular structure and its inner cavity size, the wall thickness of this particular channel-like structure is ~80 nm. The hollow nature of the structures is clearly visible in the inset of Figure 2(a), with the black arrows pointing to its corner edges.

TEM imaging and high-resolution TEM (HRTEM) imaging were performed on the molybdenum oxide structures for further characterisation and analysis. For TEM studies, the deposits were removed from the probe and dispersed on a TEM grid using methanol. HRTEM was employed to characterise the structure of the Mo-based microchannels. HRTEM performed on the grown material reveals the uniform and highly ordered crystal structure, as shown in Figure 2(b).

It can also be observed that the wall of the rectangular whisker is free of dislocations and structural defects. A lattice spacing of 0.36 nm was measured, which is close to $(\bar{1}11)$ plane of a monoclinic MoO_2 cell. SAED pattern in Figure 2(c) confirms the high degree of crystallinity of the material by showing a regular pattern of diffraction spots. EDS analysis performed on the molybdenum oxide structures (Figure 2c) shows the presence of molybdenum, oxygen and carbon. The carbon readings are attributed to the carbon tape used to hold the probe in place, and the presence of molybdenum and oxygen further confirms that the material is, in fact, an oxide of molybdenum.

3.2. *Synthesis of Fe-oxide nanorods*

Iron has a moderate melting temperature and the same cubic crystal structure as Mo and W. The introduction of iron probes in the flame medium resulted in the formation of a thin layer of material coating on the upper surface of the probe, as shown in Figure 3(a).

Figure 3(a) represents a SEM image collected on the surface of a 1 mm diameter Fe probe exposed to the flame at a height of $Z = 10$ mm. The formed coat had a characteristic brownish colour typical for iron oxide deposits. Higher resolution SEM imaging analysis revealed that the materials formed are composed of elongated 1D nanostructures characterised by high aspect ratios (Figures 3a–d). The diameters of the iron oxide nanorods vary from 10–100 nm with a typical length of a few microns. It can be observed from the SEM analysis that among the straight and uniform iron oxide structures, nanostructures with complex morphologies is also synthesised. The bending phenomena present in the structures is highlighted by the arrows in Figure 3(b). Some of the structures also appear to be branched out in T- and Y-shapes (Figure 3b–d). In the

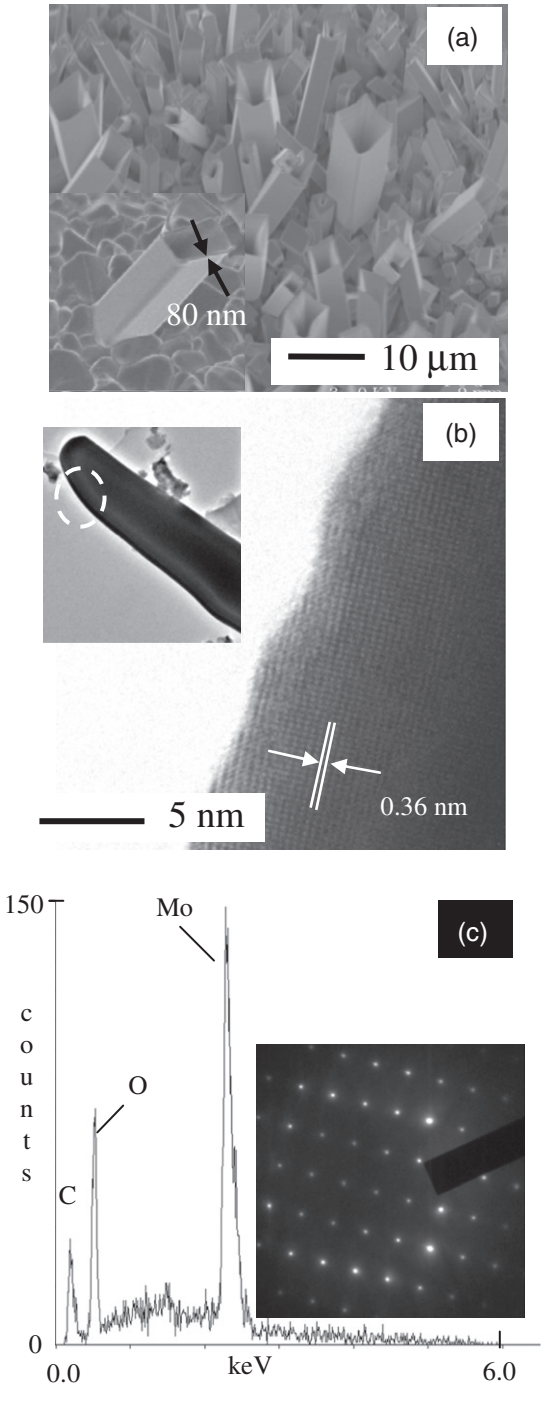

Figure 2. Molybdenum oxide hollow channels: (a) SEM image of the as-synthesized microstructures; (b) HRTEM image showing highly ordered crystalline lattice (from circled area in inset) and (c) EDS analysis and diffraction pattern.

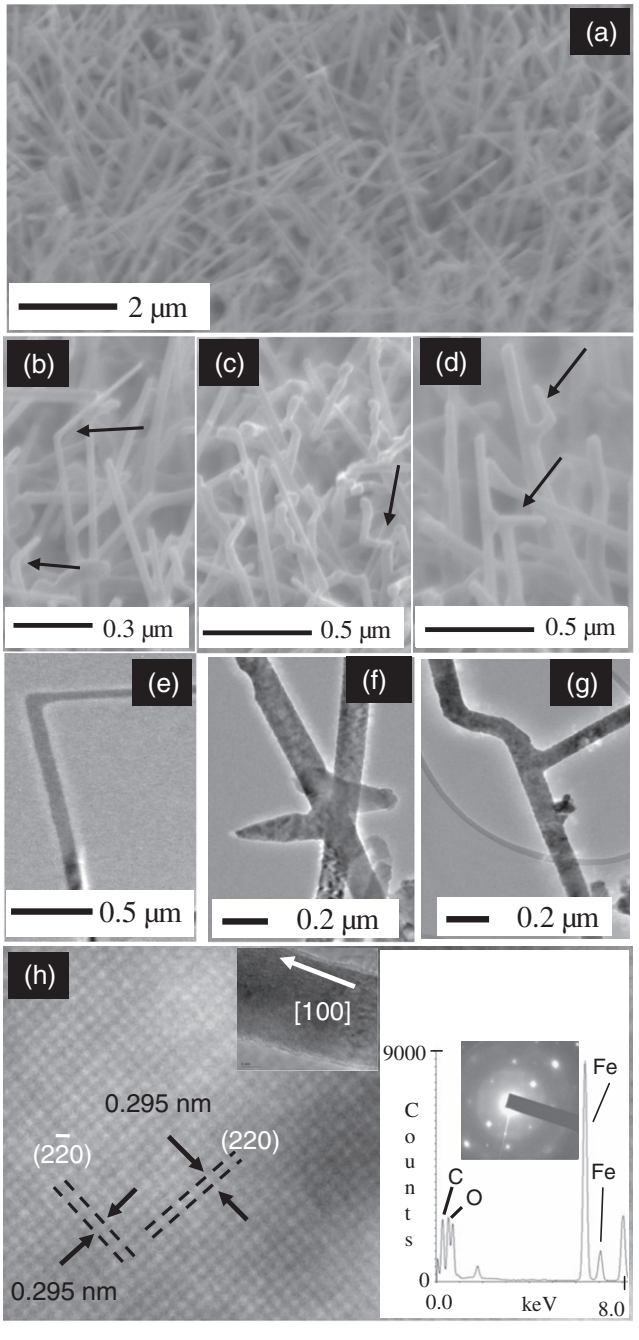

Figure 3. Iron oxide nanorods: (a–d) SEM image of as-synthesised nanorods with bending and branching phenomena as highlighted with arrows; (e–g) TEM images further illustrating bending and branching; (h) high-magnification TEM image showing highly ordered crystalline lattice (lower inset represents EDS analysis and diffraction pattern).

area of nanomaterials, the modified 'branched' and 'bent' structures are excellent candidates for fabricating composite materials with enhanced mechanical or electronic properties due to the formation of a network-like phase within the matrix. TEM and HRTEM was applied in order to provide further insights into the structure, composition and morphology of the synthesised iron-based nanorods. Representative TEM images of iron oxide nanorods are shown in Figure 3(e–h). TEM images of angled and branched iron oxide nanomaterials are shown in Figure 3(e–g). These modified structures possess the same ordered crystalline morphology as the straight nanorods. The joints in the modified structures occur abruptly, followed within a few nanometres of the joint in either direction by a uniform 1D structure. The occurrence of the branching and bending structures increases with probes positioned closer to the flame front. It is possible that bending and branching of nanowires is caused by minute temperature and flow velocity fluctuations. The highly ordered crystalline lattice of this nanorod obtained at higher magnification is displayed in Figure 3(h). Two symmetric systems of crystallographic planes each forming an angle of 45° with the nanorod axis can be clearly observed. The crystalline structure has a characteristic lattice spacing of ~0.295 nm and can be correlated with the {2 2 0} interplanar spacing of cubic magnetite (Fe_3O_4). SAED pattern in Figure 3(h) confirms the high degree of crystallinity of the material by showing a regular pattern of diffraction spots. EDS analysis performed on the iron oxide structures (Figure 3h) shows the presence of iron, oxygen and carbon.

3.3. *Synthesis of 1D W-oxide nanowires*

Molybdenum and tungsten have exceptional hardness, tensile strength and high melting points. Despite these similarities, the nanostructures formed by these metals exhibited quite distinct morphologies. The introduction of 1 mm probes made of W in the flame medium resulted in the formation of a unique 1D-type nanostructure (Figure 4). The formed nanostructures have a rod-like shape with high aspect ratios. The structural characteristics of the nanowires grown on the 1 mm diameter probe are that they are up to 50μm in length with diameters ranging from 10–100 nm. These structures are ideal candidates for gas sensing and electron emitting devices.

TEM and HRTEM performed on the grown structures of the tungsten probe revealed structural uniformity and highly ordered 1D tungsten-based nanowires. HRTEM imaging of a selected nanowire revealed that the 'core' inner dark material is a metal oxide sheathed by a 'coat' layer of carbon material as shown in Figure 4(b). HRTEM of the nanowires shows that the 'coat' is composed of a sheath of layered material with a planar spacing of 0.34 nm resembling the characteristics of graphite. HRTEM imaging of the inner 'core' dark area shows the high degree of crystallinity present. The inner metal oxide material has a lattice spacing of 0.38 nm that corresponds to (0 0 2) plane of a monoclinic WO_3. SAED pattern in Figure 4(c) confirms the high degree of crystallinity of the material by showing a regular pattern of diffraction spots. EDS analysis performed on the tungsten oxide structures (Figure 4c) shows the presence of tungsten, oxygen and carbon. The carbon readings are attributed to both the carbon tape used to hold the probe in place and to the structure itself. It is interesting to note that of all the tested transition metals in this study, only the W-oxide structures were coated with a thick layer of highly crystalline carbon. Xu et al. [35] reported that the flame synthesis of nanorods composed of W, O and traces

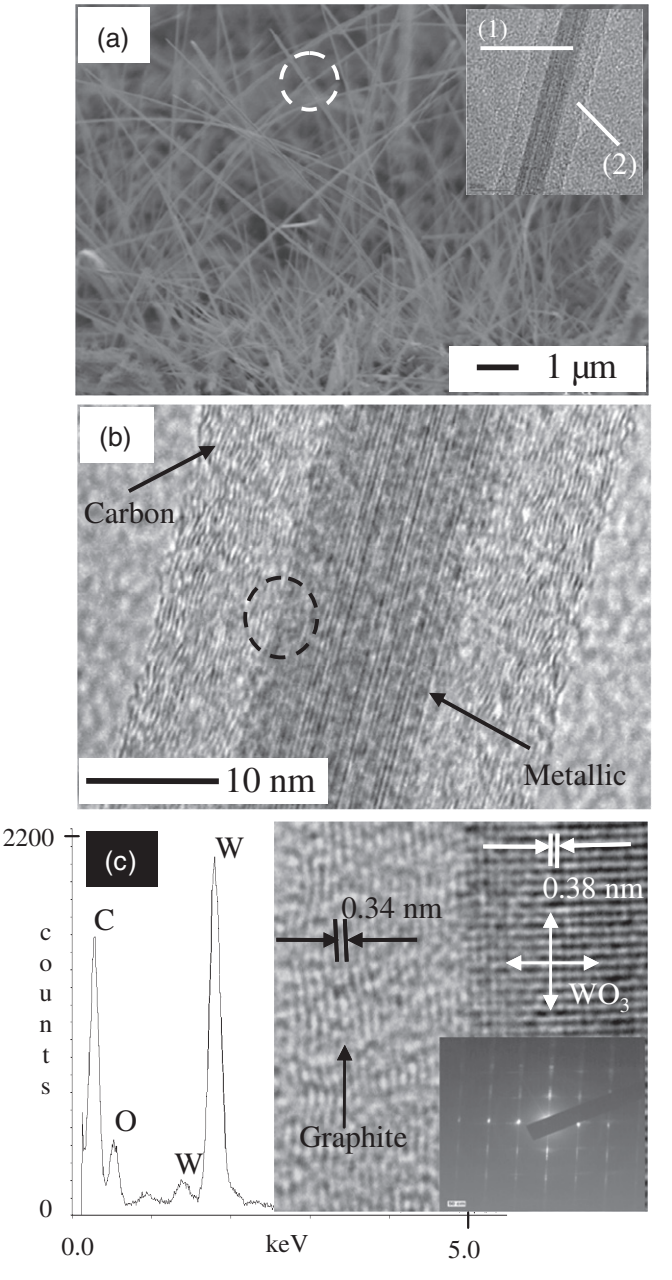

Figure 4. SEM images of tungsten - oxide nanorod layer formed on the surface of the tungsten probe: (a) low-resolution SEM showing high density of the layer, (b) HRTEM image showing straight uniform nanorods composed of two types of materials and (c) EDS conducted on a corresponding nanorod along with diffraction pattern analysis.

of C. Their results suggest that the presence of C is most likely from the deposition of C on the nanowires from carbon-containing species that diffuse from the reaction zone during the processing [35]. The application of HRTEM analysis to our products revealed that a very uniform thick layer of graphite covers the tungsten oxide nanowires. These findings merit further studies and a series of experiments are currently being conducted in our laboratories in order to obtain information on controlling the deposition/uniformity and thickness of the carbon coating layer and its formation.

4. Growth mechanism of TMOs

Experiments conducted using bulk Mo, W and Fe probes show essential similarity of the TMO synthesis process. We hypothesise that there is a common generic mechanism controlling the growth of 1D and 3D TMO structures on high-temperature probes. This mechanism involves the interaction of probe material with a flame possessing strong temperature and chemical gradients (Figure 5). In general, metal oxide/hydroxides are formed on the probe surface exposed to the high-temperature oxidative environment. These oxides/hydroxides are further evaporated and transported by the gas flow to the low-temperature side of the probe where they are reduced to other oxide forms and deposited in the form of 1D or 3D TMO materials on the upper part of the probe. This hypothetical growth mechanism is illustrated using the synthesis of Mo nanostructures. SEM analysis was performed on Mo probes exposed to the flame at several heights in order to determine a mechanism of growth for the 1D and 3D TMO structures. Figure 5 depicts the characteristic distributions for the synthesised structures on the surface of

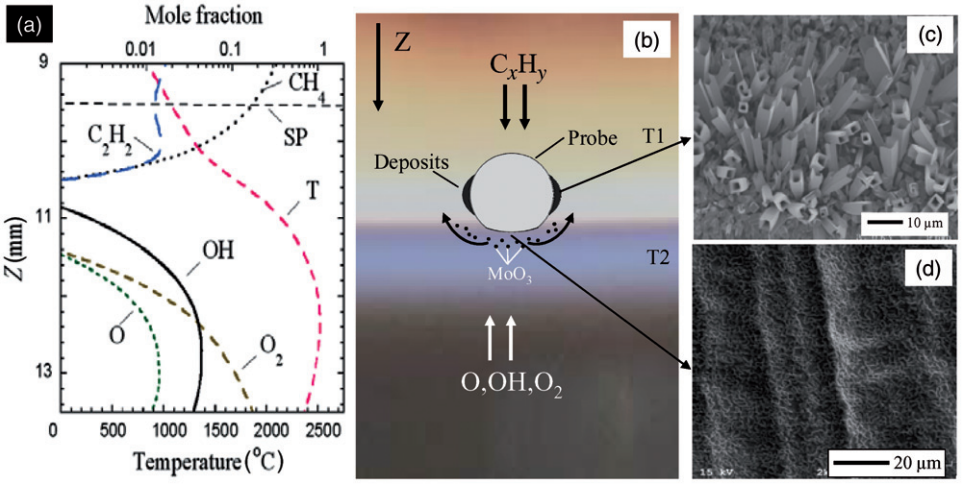

Figure 5. Schematic representation and SEM images illustrating the growth of Mo-oxide structures on the surface of a 1.0 mm diameter probe: (a) represents numerical predictions of temperature profile and distribution of major chemical species in $(96\%CH_4 + 4\%C_2H_2)/(50\%O_2 + 50\%N_2)$ flame; (b) shows probe location within the flame, material deposition location, and material transfer mechanism for a Mo probe ($T_2 > T_1$); (c) and (d) depict SEM images of the deposited layer and the engraved bottom surface of the probe, respectively.

a 1 mm diameter Mo probe. Figures 5(c) and (d) show SEM images of the formed Mo-oxide layer from the lateral surfaces and the engraved surface exposed to the oxidiser stream, respectively. The observed distribution of the deposited structures suggests the transfer of the building material by gas flow from the side of the probe exposed to the high-temperature oxidising environment and their further deposition and crystallisation on the probe surfaces downstream at an area of lower temperatures, as observed in Figure 5(b). Molybdenum probes that have been exposed to the flame contain a particular loss of symmetry in the cross-sectional area at the bottom region of the probe. Figure 5(d) depicts the engraved surface where the material has been removed due to the high-temperature oxidising environment.

As the probe is inserted in the flame medium, a layer of MoO_2 is formed on the surface of the probe facing the oxidiser side, followed by a layer composed of several molybdenum oxides, Mo_xO_{3x-1}, and finally by an outermost layer of MoO_3 [36]. At a flame position of $Z = 12$ and 11 mm, the probes are exposed to flame temperatures of 2500 and 2100°C, respectively. MoO_3 is a relatively volatile compound with a melting point of 795°C and evaporation temperature of 1155°C. As a result, MoO_3 is easily evaporated. The gas flow transports the evaporated MoO_3 along the probe surface. Its deposition downstream is a consequence of two main factors: the lower temperature of the medium and the change of the chemical species composition in this area of the flame. At the flame heights of $Z = 12$ and 11 mm, a flame temperature difference of ~400°C exists (Figure 5a). However, through the application of an optical pyrometer, the temperature of the 1 mm diameter wire was measured at flame heights of $Z = 12$ and $Z = 11$ mm as 1200°C and 1150°C, respectively. It is significant to note that the temperature of the wire is always lower than the local flame temperature due to high radiative heat losses and the thermal conductivity of the molybdenum probe. Nevertheless, flame temperature drop (Figure 5a) along the probe surface can be sufficient to generate the condensation of the evaporated oxides.

Crystallisation consists of two processes: nucleation and crystal growth. In our previous article, we presented detailed information on the nucleation process of the flame-formed rectangular hollow structures [37]. The flame-synthesised TMO products possess either a rectangular or cylindrical shape and can exhibit solid or hollow morphologies, as shown earlier. The preferential growth and formation of new crystal faces play a key role in the formation of slender prismatic whisker structures [38,39]. It is well established that the morphology of a crystal is governed by the chains of strong bonds running through the structure known as the periodic bond chain (PBC) vector [39]. The faces of a crystal are divided into three groups: (1) flat F-faces that are parallel to at least two PBC vectors and are dominant, (2) stepped S-faces that are parallel to at least one PBC vector and are of medium importance and (3) kinked K-faces which are not parallel to any PBC vector and are less frequent or do not occur at all (schematic representation is given in Figure 6) [39].

The whisker growth usually occurs at low degrees of supersaturation in a gas phase. In this case, nucleation occurs preferentially along the PBC vector characterised by the highest bonding energy producing a greatly accelerated growth rate in one direction. This leads to the prismatic crystal growth in one direction resulting in a needle-like rectangular or cylindrical shape. In the case of MoO_2, the PBC vector coincides with the lattice vector $\boldsymbol{a}$ directed along the whisker axis. As a result, the islands of new material are easily formed on the tip of the growing prismatic structures as pointed out by the arrows on

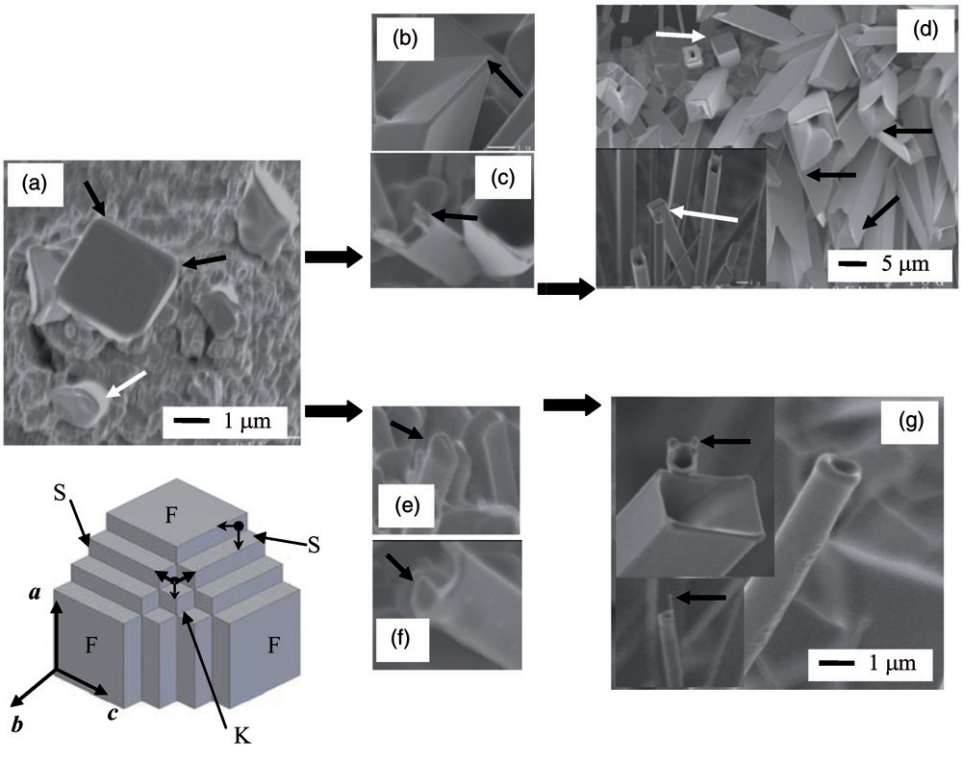

Figure 6. Schematic representation of a hypothetical whisker showing F, S and K faces. The PBC vector representing highest bonding energy is directed along the lattice vector ***a.*** Scanning electron microscope images showing preferential attachment of the material to the growing tips of solid circular and rectangular whiskers. The transformation to hollow structures occurs by dominant edge and vertex growth due to the Berg effect.

Figure 6(a)–(g). Figure 6(a) highlights the earlier stage formation of a rectangular and cylindrical structure as pointed out by the black and white arrows, respectively.

In the case of diffusion-limited growth, the Berg effect limits supply of the materials to the axial zone of the growing structures. A preferential growth on the tip boundaries leads to the formation of hollow crystals and leaf-like structures. The diffusion-limited preferential growth can be easily observed in the earlier formation stage of MoO_2 products (Figure 6b, c, e, f). The crystals have protruding corners. Figure 6(b) shows the earlier stage of the formation of hollow crystals by the preferential growth occurring along one of the edges of the rectangular structures, as highlighted by the arrow. The preferential growth at the tip of the cylindrical structure is evident in Figure 6(e), one side is longer than the other, as shown by the arrow. During the diffusion-controlled growth, the structures continue their growth along the edges creating a hollow morphology, as the influx material may never reach the centre. Figure 6(c) and (f) represents the intermediate growth stage of hollow rectangular and cylindrical structures, respectively. Fully developed rectangular and cylindrical hollow structures are shown in Figure 6(d) and (g). Figure 6(d) also shows that within the many hollow structures, a few solid structures can co-exist as pointed out by the

white arrows. The tips of the solid structures are completely flat supporting our hypothesis that an earlier preferential growth is essential for the structures to become hollow.

In the case of oxide crystals, it has been shown that the addition of small percentages of transition metal oxide impurities (i.e. Fe_2O_3) can enhance the formation of hollow needle crystals [39]. In our studies, we have observed that W- and Fe-oxides are solid 1D nanostructures. In the case of Mo, the majority of the synthesised structures are hollow.

5. Conclusions

We report the formation of molybdenum-, iron- and tungsten-oxide nanostructures with unique structural morphologies using the novel flame gradient synthesis method. Probes are inserted in an opposed-flow flame formed by streams of fuel (96% $CH_4 + 4\%$ C_2H_2) and oxidiser (50% $O_2 + 50\%$ N_2).

The insertion of 1 mm diameter molybdenum probe resulted in the synthesis of metal oxide structures with rectangular and cylindrical shapes. The structures can be solid or hollow. Iron oxide nanorods with diameters ranging from 10 to 100 nm and of a few microns in length are grown on the surface of the iron probe facing the fuel side, forming a dense coating layer. T- and Y-branching structures are frequently observed within the straight nanorods. 1D tungsten oxide elongated structures with needle-like shapes were synthesised using high-purity W probes. The morphological characteristics of the nanowires grown on the 1 mm diameter tungsten probe include lengths up to 50μm and nanoscale diameters ranging from 10 to 100 nm. The nanowires have a composite structure with an inner core crystalline metal oxide material covered by an outer sheath layer of well-ordered carbon.

All tested probes show the oxidation and transfer of metal oxide material from the lower to the upper part of the probe. The proposed generic growth mechanism for TMO structures consists of transferring metal oxides/hydroxides from the high- to low-temperature side of the probe where the species are reduced and crystallised in the form of metal oxide nanostructures.

Acknowledgements

The authors would like to extend special thanks to Dr. Alan Nicholls and Ms. Kristina Jarosius from the UIC Research Resource Center for assistance in SEM and TEM studies, encouragement and helpful discussion. We would also like to thank Mr. Gregory Strout from the Samuel Roberts Noble Electron Microscopy Laboratory at the University of Oklahoma for help with high resolution studies on the JEOL-2010F field emission TEM. The support of this work by the National Science Foundation through the Collaborative Research Grants; CTS-0854433 and CTS-0854006 is gratefully acknowledged.

References

[1] W.J. Grieco, J.B. Howard, C.L. Rainey, and J.B.V. Sande, *Fullerenic carbon in combustion-generated soot*, Carbon 38 (2000), pp. 597–614.

[2] M. Silvestrini, W. Merchan-Merchan, H. Richter, A. Saveliev, and L.A. Kennedy, *Fullerene formation in atmospheric pressure opposed flow oxy-flames*, Proc. Combust. Inst. 30 (2005), pp. 2545–2552.
[3] J.B. Howard, D.K. Chowdhury, and J.B. Vander Sande, *Carbon shell in flames*, Nature 370 (1994), p. 603.
[4] L. Yuan, K. Saito, and W.Z. Hu, *Ethylene flame synthesis of well-aligned multi-walled carbon nanotubes*, Chem. Phys. Lett. 346 (2001), pp. 23–28.
[5] L. Yuan, K. Saito, C. Pan, F.A. Williams, and A.S. Gordon, *Nanotubes from methane flames*, Chem. Phys. Lett. 340 (2001), pp. 237–241.
[6] T.X. Li, K. Kuwana, K. Saito, H. Zhang, and Z. Chen, *Temperature and carbon source effects on methane–air flame synthesis of CNTs*, Proc. Combust. Inst. 32 (2009), pp. 1855–1861.
[7] R.L. Vander Wal, *Flame synthesis of Ni-catalyzed nanofibers*, Carbon 40 (2002), pp. 2101–2107.
[8] R.L. Vander Wal, *Flame synthesis of substrate-support metal catalyzed carbon nanotubes*, Chem. Phys. Lett. 324 (2000), pp. 217–223.
[9] R.L. Vander Wal, *Fe-catalyzed single-walled carbon nanotubes synthesis within a flame environment*, Combust. Flame 130 (2002), pp. 37–47.
[10] K. Okada, S. Komatsu, T. Ishigaki, S. Matsumoto, and Y. Moriyoshi, *Spontaneous growth of whiskers from an interlayer of Mo_2C beneath a diamond particle deposited in a combustion-flame*, J. Cryst. Growth 116 (1992), pp. 307–313.
[11] F. Xu, X. Liu, and S.D. Tse, *Synthesis of carbon nanotubes on metal alloy substrates with voltage bias in methane inverse diffusion flames*, Carbon 44 (2006), pp. 570–577.
[12] G.W. Lee, J. Jurng, and J. Hwang, *Formation of Ni-catalyzed multiwalled carbon nanotubes and nanofibers on a substrate using an ethylene inverse diffusion flame*, Combust. Flame 139 (2004), pp. 167–175.
[13] M. Suemitsu, T. Abe, H.J. Na, and H. Yamane, *MoO_2 hollow fiber with rectangular cross sections*, Jpn. J. Appl. Phys. 44 (2005), pp. L449–L450.
[14] N.A. Dhas and A. Gedanken, *Sonochemical synthesis of molybdenum oxide- and molybdenum carbide-silica nanocomposites*, Chem. Mater. 9 (1997), pp. 3144–3154.
[15] M. Anpo, M. Kondo, Y. Kubokawa, C. Louis, and M. Che, *Dynamic studies of the photoinduced metathesis of C_3H_6 and photoreduction of Mo with CO on anchored and impregnated Mo/SiO_2 catalysts*, J. Chem. Soc. Faraday Trans. 1 84 (1988), pp. 2771–2782.
[16] Y. Liu, Y. Qian, M. Zhang, Z. Chen, and C. Wang, *Preparation of nano-sized amorphous molybdenum dioxide powders by use of γ-ray radiation method*, Mater. Res. Bull. 31 (1996), pp. 1029–1033.
[17] W. Merchan-Merchan, A.V. Saveliev, and A.M. Taylor, *High rate flame synthesis of highly crystalline iron oxide nanorods*, Nanotechnology 19 (2008), pp. 125605–125609.
[18] F. Xu, X. Liu, S.D. Tse, F. Cosandey, and B.H. Kear, *Flame synthesis of zinc oxide nanowires*, Chem. Phys. Lett. 449 (2007), pp. 175–181.
[19] P.M. Rao and X. Zheng, *Rapid flame synthesis of α-Fe_2O_3 nanoflakes and CuO nanoneedles*, Proceedings of the 6th US National Combustion Meeting, May 17–20 Ann Arbor. Michigan (2009).
[20] J. Zhou, N.S. Xu, S.Z. Deng, J. Chen, and J.C. She, *Synthesis of large-scaled MoO_2 nanowire arrays*, Chem. Phys. Lett. 382 (2003), pp. 443–446.
[21] C.J. Jia, L.D. Sun, Z.G. Yan, L.P. You, F. Luo, X.D. Han, Y.C. Pang, Z. Zhang, and C.H. Yan, *Single-crystalline iron oxide nanotubes*, Angew. Chem. Int. Ed. 44 (2005), pp. 4328–4333.
[22] L. Vayssieres, N. Beermann, S.E. Lindquist, and A. Hagfeldt, *Controlled aqueous chemical growth of oriented three-dimensional crystalline nanorod arrays: Application to iron (III) oxides*, Chem. Mater. 13 (2001), pp. 233–235.

[23] S. Chen, J. Feng, X. Guo, J. Hong, and W. Ding, *One-step wet chemistry for preparation of magnetite nanorods*, Mater. Lett. 59 (2005), pp. 985–988.
[24] R.M. Cornell and U. Schwertmann, *The Iron Oxides: Structure, Properties, Reactions, Occurrence and Uses*, Wiley-VCH, New York, 1996.
[25] T.A. Crowley, K.J. Ziegler, D.M. Lyons, D. Erts, O. Hakan, M.A. Morris, and J.A. Holmes, *Synthesis of metal and metal oxide nanowire and nanotube arrays within a mesoporous silica template*, Chem. Mater. 15 (2003), pp. 3518–3522.
[26] D.S. Xue, C.X. Gao, Q.F. Liu, and L.Y. Zhang, *Preparation and characterization of hematite nanowire arrays*, J. Phys. Condens. Matter 15 (2003), pp. 1455–1459.
[27] C. Terrier, M. Abid, C. Arm, S. Serrano-Guisan, L. Gravier, and J.P. Anserment, *Fe_3O_4 nanowires synthesized by electroprecipitation in templates*, J. Appl. Phys. 98 (2005), pp. 086102-1–086102-3.
[28] Y. Ding, J.R. Morber, R.L. Snyder, and Z.L. Wang, *Nanowire structural evolution from Fe_3O_4 to e-Fe_2O_3*, Adv. Funct. Mater. 17 (2007), pp. 1172–1178.
[29] L. Chi, N. Xu, S. Deng, J. Chen, and J. She, *An approach for synthesizing various types of tungsten oxide nanostructures*, Nanotechnology 17 (2006), pp. 5590–5595.
[30] Z. Liu, D. Zhang, S. Han, C. Li, B. Lei, W. Lu, J. Fang, and C. Zhou, *Single crystalline magnetite nanotubes*, J. Am. Chem. Soc. 127 (2005), pp. 6–7.
[31] J.R. Morber, Y. Ding, M.S. Haluska, Y. Li, J.P. Liu, Z.L. Wang, and R.L. Snyder, *PLD-assisted VLS growth of aligned ferrite nanorods, nanowires, and nanobelts synthesis, and properties*, J. Phys. Chem. B. 110 (2006), pp. 21672–21679.
[32] J. Stringer, *Oxidation of tantalum in oxygen-nitrogen and oxygen-inert gas mixtures*, Oxid. Met. 11 (1977), pp. 225–239.
[33] K. Ogata, K. Maejima, S.Z. Fujita, and S.G. Fujita, *Growth mode control of ZnO toward nanorod structures or high-quality layered structures by metal-organic vapor phase epitaxy*, J. Cryst. Growth 248 (2003), pp. 25–30.
[34] A. Beltrame, P. Porshnev, W. Merchan-Merchan, A. Saveliev, A. Fridman, L.A. Kennedy, O. Petrova, S. Zhdanok, F. Amoury, and O. Charon, *Soot and NO formation in methane oxygen enriched diffusion flames*, Combust. Flame 124 (2001), pp. 295–310.
[35] F. Xu, S.D. Tse, J.F. Al-Sharab, and B.H. Kear, *Flame synthesis of aligned tungsten oxide nanowires*, Appl. Phys. Lett. 88 (2006), p. 243115.
[36] T. Saburi, H. Murata, T. Suzuki, Y. Fujii, and K. Kiuchi, *Oxygen plasma interactions with molybdenum: Formation of volatile molybdenum oxides*, J. Plasma Fusion Res. 78 (2002), pp. 3–4.
[37] W. Merchan-Merchan, A.V. Saveliev, and A. Taylor, *Nucleation and growth mechanism for flame synthesis of MoO_2 hollow microchannels with nanometer wall thickness*, Micron 40 (2009), pp. 821–826.
[38] I. Sunagawa, *Crystals, Growth, Morphology and Perfection*, Cambridge University Press, Cambridge, 2005, pp. 72–75.
[39] P. Hartman and W.G. Perdok, *On the relations between structure and morphology of crystals-I*, Acta Cryst. 8 (1955), pp. 49–52.